MAUSAM, 52, 1(January 2001), 133-150

551.513 : 551.553.21 (540)

Observed and model simulated interannual variability of the Indian monsoon

V. KRISHNAMURTHY and J. SHUKLA

Center for Ocean-Land-Atmosphere Studies,

Institute of Global Environment and Society, Inc.

4041 Powder Mill Road, Suite 302,

Calverton, MD 20705, USA

सार - 1979 - 98 वर्षों के प्रक्षित विश्वस्तरीय समुद्र सतह तापमान (एस.एस.टी.) के साथ समुद्र भू वायुमंडल (सी.ओ.एल.ए.) केन्द्र सामान्य परिचालन निदर्श का सात बार समाकलन किया गया है। निदर्श अनुकारित वार्षिक चक्र, मौसमी माध्य और ग्रीष्म कालीन मानसून वर्षा की अंतः वार्षिक विभिन्नताओं और भारतीय क्षेत्र में इनके परिसंचरण की तुलना बाद में लिए गए प्रेक्षणों के साथ की गई है। यह देखा गया है कि यद्यपि इस निदर्श को उष्णकटिबंधी एस.एस.टी. की विसंगतियों के स्थानीय और विश्वस्तरीय अनुक्रिया के अनुकरण में असाधारण सफलता मिली है तथापि भारत में मानसून वर्षा की अंतः वार्षिक विभिन्नताओं का अनुकरण करने की इस निदर्श में कम क्षमता पाई गई है। यह सच है कि तत्काल हाल के बीस वर्षों में प्रेक्षित उष्णकटिबंधी स्थिर एस.एस.टी. और भारतीय ग्रीष्म मानसून वर्षा के मध्य पाए गए सहसंबंध इसके पहले के बीस वर्षों के मध्य के संहसंबंधों की तुलना में न्यून पाए गए है। भारत में वर्षा की विभिन्नताओं का अनुकरण करने विशेषकर समुद्री क्षेत्रों में जलवायु विज्ञान मानसून परिसंचरण का अनुकरण करने में इस निदर्श की असमर्थता का व्यापक कारण संभवतः निदर्श की क्रमबद्ध त्रुटियाँ ही हैं।

ABSTRACT . The Center for Ocean-Land-Atmosphere (COLA) general circulation model has been integrated seven times with observed global sea surface temperature (SST) for the years 1979–98. The model-simulated annual cycle, the seasonal mean and the interannual variability of the summer monsoon rainfall and circulation over the Indian region are compared with the corresponding observations. It is found that, although this model has shown remarkable success in simulating the local and global response of tropical SST anomalies, the model shows poor skill in simulating the interannual variability of monsoon rainfall over India. While it is true that the correlation between the observed tropical Pacific SST and the Indian summer monsoon rainfall for the most recent 20 years itself is considerably lower than that for other 20-year periods in the past, it is likely that the model's inability to simulate rainfall variability over India is largely related to the systematic errors of the model in simulating the climatological mean monsoon circulation and rainfall, especially over the oceanic regions.

Key words – Monsoon modeling, GCM simulation of monsoon rainfall, SST-monsoon relation.

1. Introduction

Atmospheric general circulation models (AGCMs) are an important tool to simulate the present climate, to predict the future climate and to conduct numerical experiments to understand the mechanisms of climate variability and its predictability (Sperber and Palmer 1996). The ability of an AGCM to predict climate variations depends on the model's ability to simulate the mean climate and its space-time variability (Webster *et al.* 1998). The COLA AGCM, described in the next section, has been used for large number of sensitivity and predictability studies. In particular, the model which is being used extensively to study the predictability of the Asian summer monsoon has shown remarkable success in simulating the global effect of tropical SST anomalies (Shukla 1998). This paper presents an account of the ability and limitations of the COLA AGCM in simulating the Asian summer monsoon circulation and rainfall including its interannual variability. In most of the numerical simulation studies, different realizations of the same model are compared to investigate the model's sensitivity to changes in the initial or boundary conditions; however, in this case, all comparisons are done with respect to the corresponding observations.

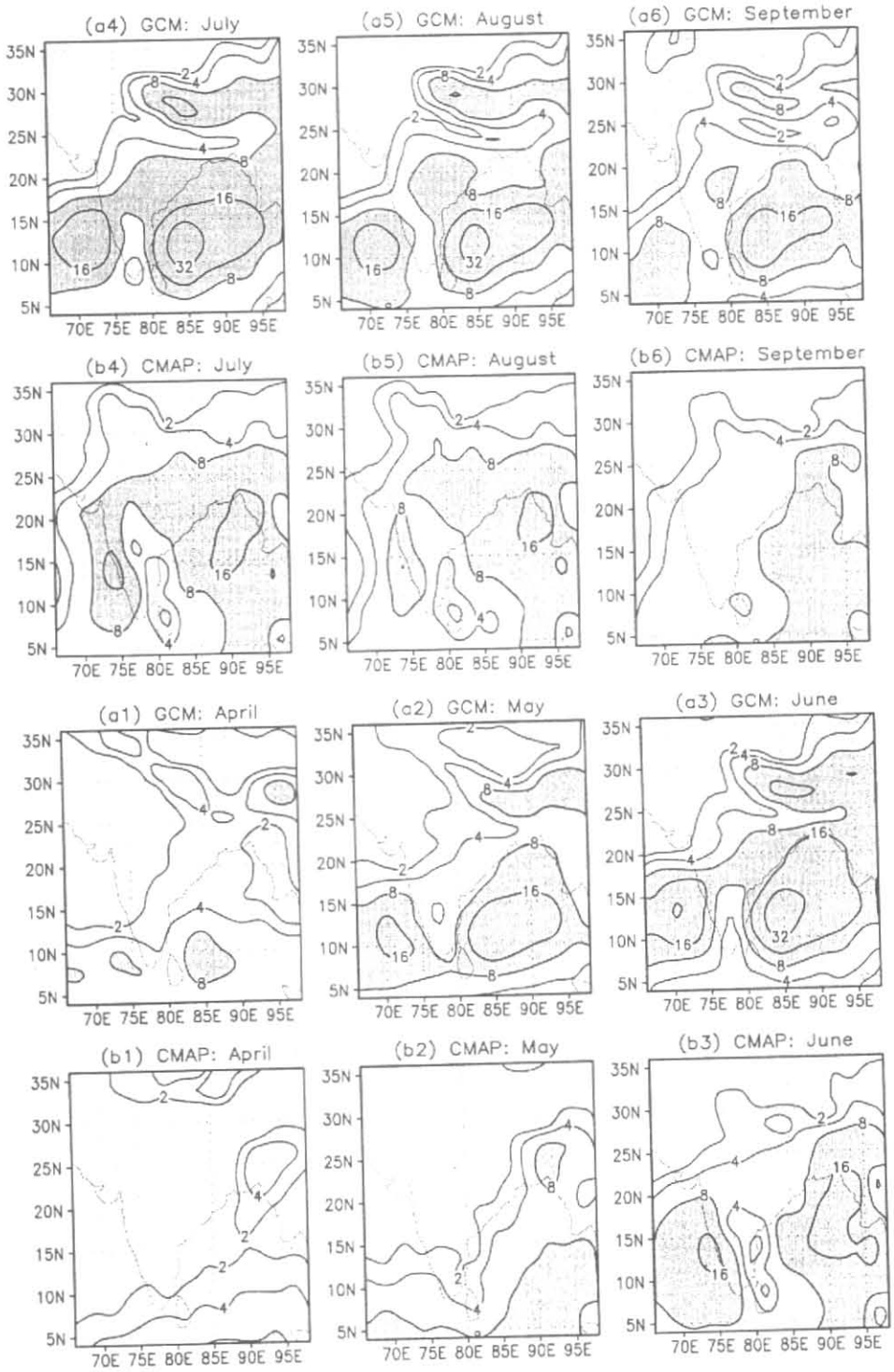

Fig. 1. Monthly rainfall climatology for (a1–a6) the ensemble mean of COLA GCM integrations and (b1–b6) the CMAP data for April to September. Both climatologies are based on 1979–98. The contours are 2, 4, 8 16 and 32 mm day^{-1}, and contours > 8 are shaded

2. Model and data

2.1. *COLA Model and experiments*

The COLA atmospheric general circulation model (AGCM) used in this study is a global spectral model with rhomboidal truncation at zonal wavenumber 40 (Kinter *et al.* 1997). The Gaussian grid associated with this truncation has 128 points in the longitudinal direction and 102 points in the latitudinal direction, and the vertical structure is represented by 18 unevenly spaced levels in sigma coordinate. This version of the model includes a dynamical core that is based on an earlier version of the operational medium range forecast model of the National Centers for Environmental Prediction (NCEP) (NMC 1988) and modifications of the subgrid scale physical parameterizations. The model's parameterizations include solar and terrestrial radiative heating, cloud-radiation interaction, deep convection (relaxed Arakawa-Schubert scheme), large scale condensation, shallow convection, a turbulence closure scheme for subgrid exchange of heat, momentum and moisture, and interaction between the land surface and the atmosphere (Shukla *et al.* 1999).

This paper describes the results of an ensemble of seven integrations of the COLA AGCM. The integrations were carried out from 1 January 1979 to 31 December 1998 with seven different observed global atmospheric initial conditions at 0000 UTC of each day from 26 December 1978 to 1 January 1979 produced by NCEP. The SST and sea ice data used in these integrations are based on Climate Prediction Center (CPC) weekly $1° \times 1°$ Optimum Interpolation Sea Surface Temperature (OISST) analyses. The climatology of the soil wetness analysis of the European Center for Medium Range Weather Forecasts (ECMWF) analysis-forecast system for 1987–93 was used as the initial soil wetness, and the subsequent evolution of the soil wetness fields is determined by the COLA model. The definition of the initial snow mass on land points was based on the values of albedo. The details of the boundary conditions are discussed by Shukla *et al.* (1999).

2.2. *Observed data*

The observed precipitation data used in this study come from different sources. The first dataset consists of daily rainfall at more than 3700 rain gauge stations maintained by the India Meteorological Department (IMD) over land in India. These data, available at the National Center for Atmospheric Research (NCAR) for the period 1901–70, were placed on a $1° \times 1°$ grid over India by Hartman and Michelsen (1989) and will be referred to as the IMD dataset. The second dataset consisting of monthly mean all-India rainfall, constructed by Parthasarathy *et al.* (1995), is based on observations at 306 uniformly distributed land stations over India and has been updated to cover the period 1871–1998. The third dataset is the CPC merged analysis of precipitation (CMAP) with global monthly mean precipitation for 1979–98 (Xie and Arkin 1996). The fourth dataset consists of monthly mean rainfall estimates from the Microwave Sounding Unit (MSU) measurements available only over the oceans for 1979–93 (Spencer 1993). The fifth dataset is the monthly precipitation climatology of Legates and Willmott (1990) based on the period 1960–90 and reinterpolated on a global $0.5° \times 0.5°$ grid by Willmott. As a proxy for precipitation, National Oceanic and Atmospheric Administration (NOAA) interpolated outgoing longwave radiation (OLR) data for 1979–98 were obtained from the NOAA-CIRES Climate Diagnostics Center, Boulder, Colorado.

The circulation data used in this study are the products of NCEP-NCAR reanalysis project (Kalnay *et al.* 1996) based on a state-of-the-art global data assimilation system that remains unchanged throughout the reanalysis period. Monthly mean horizontal winds and vertical velocity at standard pressure levels were obtained for the period 1979-98. Monthly mean precipitation data from the reanalysis project were also used.

3. Annual cycle and seasonal means

From the seven ensemble integrations of the model, the ensemble mean of the monthly means of various fields were calculated for the period 1979–98. In this section, the climatology of precipitation and circulation fields of the ensemble mean of the model integrations are discussed and comparisons with corresponding fields from the observed data are made.

3.1. *Monthly precipitation over India*

The monthly rainfall climatology of the model's ensemble mean rainfall over the Indian region for April–September is shown in Fig. 1 along with the rainfall climatology of observed CMAP data for 1979–98. Although the general structure of the observed rainfall climatology is present in the model climatology, there are also noticeable differences. In the model simulation, the onset of the monsoon occurs in April and most of India is covered with significant amount of rainfall (2–8 mm day^{-1}) during May, occurring at least a month earlier than observed. The rainfall over the Bay of Bengal and the Arabian Sea is substantially higher in the model climatology during May – September. The rainfall

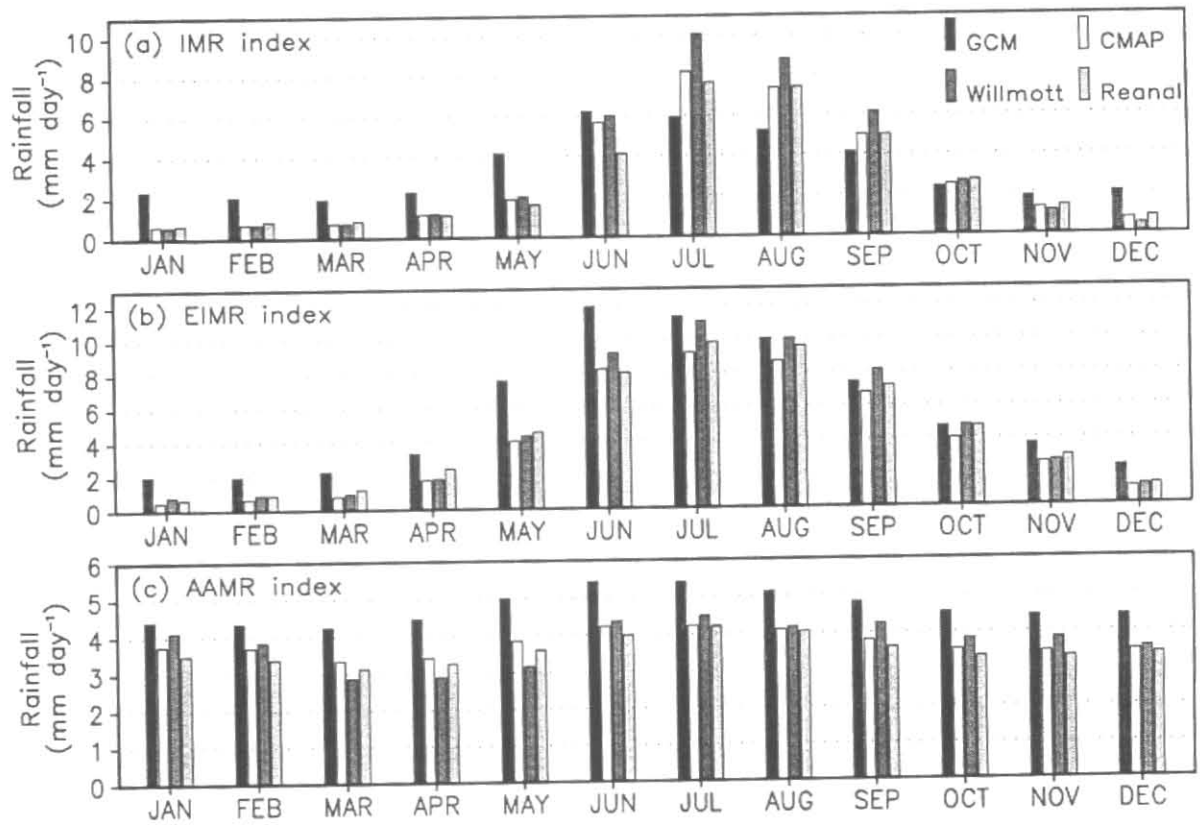

Figs. 2(a-c). Annual cycle from the monthly climatologies (mm day^{-1}) of (a) IMR index, (b) EIMR index and (c) AAMR index for the ensemble mean of COLA GCM integrations and for observed datasets of CMAP, Willmott and NCEP-NCAR reanalysis

maximum over the Bay of Bengal is shifted southeastward compared to the CMAP climatology. Over land in India, the model produces more rainfall during June, but produces a comparable amount of rainfall during July and August as the CMAP climatology. In September, the model's rainfall is slightly higher over both land and surrounding ocean.

3.2. *Annual cycle of rainfall indices*

To compare the annual cycle of the rainfall climatology of the model simulation with the observations over different regions of the Asian-Australian monsoon region, three rainfall indices are defined: (*i*) the Indian monsoon rainfall (IMR) index is the area-averaged rainfall over the land region of India; (*ii*) the extended Indian monsoon rainfall (EIMR) index is the area-averaged rainfall over (70°–110°E, 10°–30°N) as defined by Goswami *et al.* (1999) and covering the oceanic region around India; and (*iii*) the Asian-Australian monsoon rainfall (AAMR) index is the area-averaged rainfall over (40°–160°E, 40°S–40°N). The annual cycle of the three rainfall indices obtained from the monthly climatology are shown in Fig. 2 for the ensemble mean of the model integrations and for the observed rainfall from CMAP, NCEP-NCAR reanalysis and Willmott climatology. The observed data shown in Fig. 2 cover both land and ocean over the regions considered. The CMAP and NCEP-NCAR reanalysis climatologies are based on 1979–98 and the Willmott climatology is based on 1960–90.

The IMR index shows general agreement among the three observed datasets except for slight differences during June-September (Fig. 2). The IMR of NCEP-NCAR reanalysis is very close to that of the CMAP for all months except for a slightly lower value in June. However, both CMAP and NCEP-NCAR datasets underestimate the IMR for July–September by 1–2 mm day^{-1} compared to the Willmott climatology. In order to get a more precise comparison, the actual values of the monthly IMR index are provided in Table 1 for the climatologies of model ensemble mean and the observed data from IMD, Parthasarathy, CMAP and Willmott. Since the IMD and Willmott climatologies are based on large number of

TABLE 1

IMR index (mm day^{-1}) of monthly climatology, JJAS seasonal climatology and annual climatology of IMD, Parthasarathy, Willmott, CMAP and ensemble mean of COLA GCM integrations

Period	IMD	Parthasarathy	Willmott	CMAP	COLA GCM
January	0.46	0.36	0.59	0.63	2.35
February	0.51	0.45	0.68	0.73	2.05
March	0.51	0.49	0.72	0.72	1.90
April	0.86	0.88	1.17	1.13	2.25
May	1.69	1.69	2.00	1.91	4.15
June	5.70	5.45	6.01	5.64	6.22
July	9.98	8.85	10.07	8.14	5.90
August	8.49	7.86	8.83	7.31	5.23
September	6.00	5.70	6.13	4.88	4.10
October	2.72	2.49	2.61	2.41	2.35
November	1.22	1.05	1.11	1.20	1.83
December	0.45	0.38	0.45	0.65	2.04
JJAS	7.57	6.99	7.76	6.49	5.37
Annual	3.24	2.97	3.36	2.95	3.36

station data interpolated to a fine grid and cover different long periods of time, it is not surprising to note from Table 1 that the IMR index is very close for the two datasets. The IMR index of Parthasarathy dataset, based on less number of stations that are uniformly placed over India for the period 1871–1998, comes very close to that of the IMD dataset except for slight underestimation during July and August. From Fig. 2(a) and Table 1, it is seen that the IMR index of the model's ensemble mean is higher for January-May and December by about 1.5–3 mm day^{-1} compared to observations, whereas it is lower by about 2–4 mm day^{-1} for July-September and quite close for June, October and November.

The EIMR index shown in Fig. 2(b) behaves similar to the IMR index (Fig. 2a) with very little rainfall during January–April, substantial rainfall during May–September and declining amount of rainfall during October–December. The EIMR index has a slightly higher value than the IMR index for all months. The difference among the three observed datasets is small for the EIMR index. It is remarkable that the NCEP-NCAR reanalysis has estimated the IMR and EIMR indices as skillfully as the CMAP dataset. The EIMR index of the monthly climatology of the model's ensemble mean is consistently higher for all months, with differences of up to 4 mm day^{-1} during May and June. This is primarily because the simulated rainfall over the Bay of Bengal and the Arabian Sea for May and June is higher than the corresponding observations. The model's EIMR index is somewhat closer to the observed values during July–September. From Figs. 2 (a & b), it is clear that the model climatology shows an earlier onset of monsoon over the Indian region.

The AAMR index averages the rainfall over a large region, and its value is about half of the peak value of the EIMR index. The variation of the AAMR index is small during the annual cycle. The AAMR index is quite close for the three observed datasets for all months. While the AAMR index of the climatology of the model's ensemble mean follows the same trend as the observed data, the model overestimates the index for all months with differences of 0.5–1.5 mm day^{-1}.

3.3. *Seasonal mean of precipitation*

The climatology of the summer monsoon rainfall simulated by the model over India during JJAS season is now compared with several observed datasets. The JJAS seasonal rainfall climatology of the ensemble mean of the model integrations and that of observed IMD, CMAP, NCEP-NCAR reanalysis and MSU datasets are presented in Fig. 3. The JJAS seasonal climatology of the OLR is also shown in Fig. 3. The IMD climatology is more reliable as it is based on data on a fine scale grid covering a long period of 1901–70. As discussed by Krishnamurthy and Shukla (1999), the IMD climatology (Fig. 3b) shows maxima over Central India, the Western Ghats and the

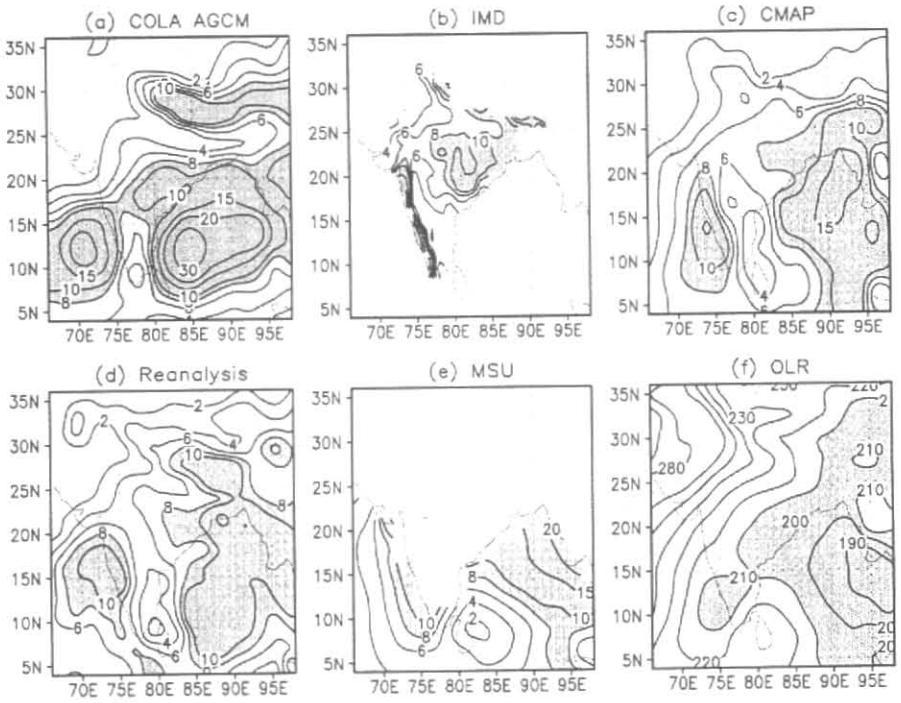

Figs. 3(a-f). JJAS seasonal rainfall climatology for (a) the ensemble mean of COLA GCM integrations, (b) IMD dataset, (c) CMAP, (d) NCEP-NCAR reanalysis and (e) MSU dataset. (f) JJAS seasonal climatology of observed OLR. All climatologies are based on 1979-98 except (b) which is based on 1901-70. In (a–e), the contours are 2, 4, 6, 8 10, 15, 20 and 30 mm day^{-1}, and contours > 8 are shaded. In (f), the contour interval is 10 W m^{-2}, and contours < 210 are shaded

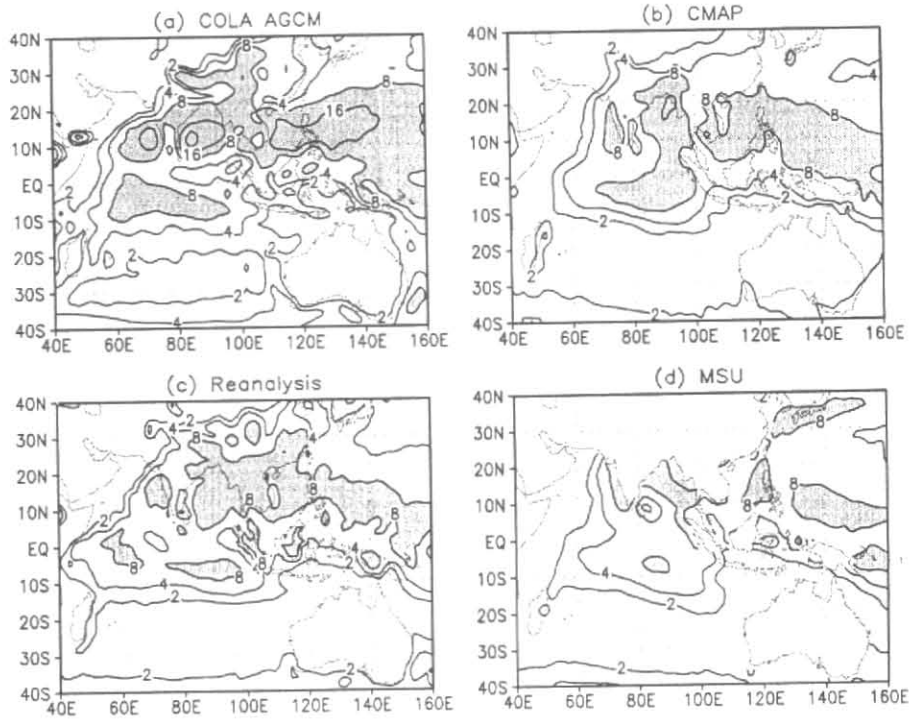

Figs. 4(a-d). JJAS seasonal rainfall climatology for (a) the ensemble mean of COLA GCM integrations, (b) CMAP, (c) NCEP-NCAR reanalysis, (d) MSU dataset. The contours are 2, 4, 8, 16, and 32 mm day^{-1}, and contours > 8 are shaded

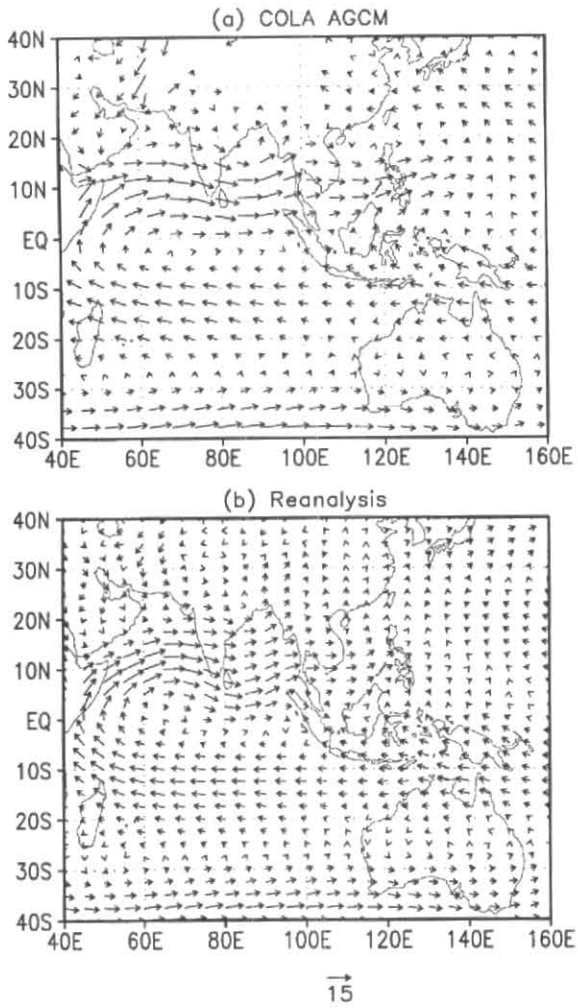

Figs. 5(a&b). JJAS seasonal climatology of the horizontal wind vector (U, V) at 850 hPa for (a) the ensemble mean of COLA GCM integrations and (b) NCEP-NCAR reanalysis. Both climatologies are based on 1979–98. The unit vector is 15 m s^{-1}. The two panels have different arrow densities because of different resolutions of the GCM and reanalysis grids

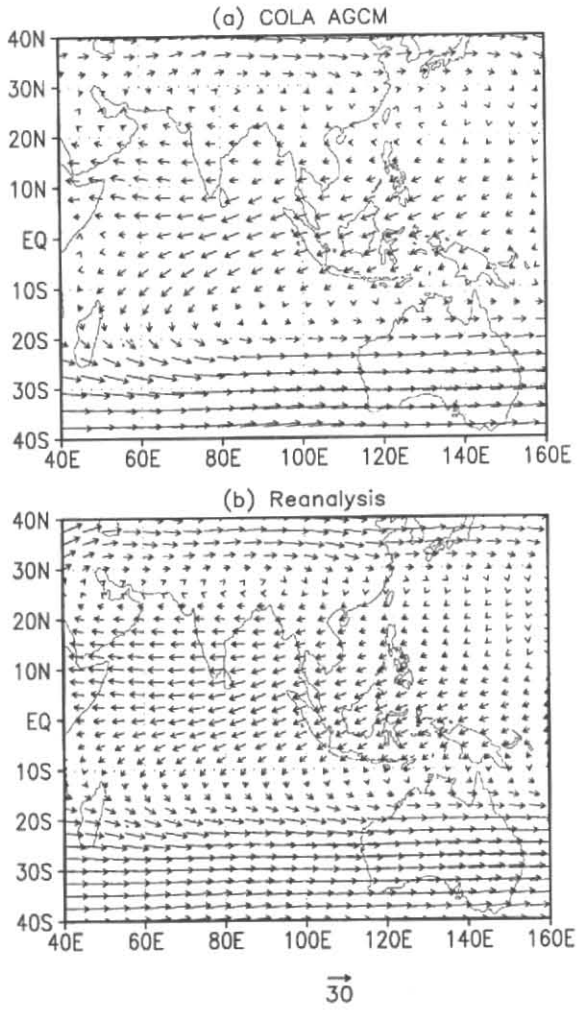

Figs 6(a&b). JJAS seasonal climatology of the horizontal wind vector (U, V) at 200 hPa for (a) the ensemble mean of COLA GCM integrations and (b) NCEP-NCAR reanalysis. Both climatologies are based on 1979–98. The unit vector is 30 m s^{-1}. The two panels have different arrow densities because of different resolutions of the GCM and reanalysis grids

hilly regions of the northeast. Although the heavy rainfall over the Western Ghats and the northeast are present, but with lower values, in the climatologies of CMAP and NCEP-NCAR reanalysis Figs. 3 (c & d), the land-locked maxima over the Central India is not as well defined in the two climatologies. The climatologies of CMAP, NCEP-NCAR reanalysis and MSU datasets Figs. 3 (c - e) have comparable structure over the Arabian Sea but differ considerably over the Bay of Bengal. The location of the maximum and the intensity are different over the Bay of Bengal for the three datasets. The climatology of the OLR (Fig. 3f) has somewhat close resemblance to the MSU climatology over the Bay of Bengal, but does not show good correspondence with other climatologies over land and Arabian Sea. It is somewhat surprising that we are as yet unable to have a reliable quantitative estimate of the location and intensity of the summer monsoon rainfall maximum.

Although the climatology of the ensemble mean of the model (Fig. 2a) captures the general features of the observed climatologies of IMD and CMAP, the location of the maxima and the intensities show differences. Over land, the model climatology shows heavy rainfall over the Western Ghats, the rainshadow in the southeast and less rainfall over the western desert. However, the maximum over the central India is shifted considerably to south compared to the IMD climatology. Over the Arabian Sea,

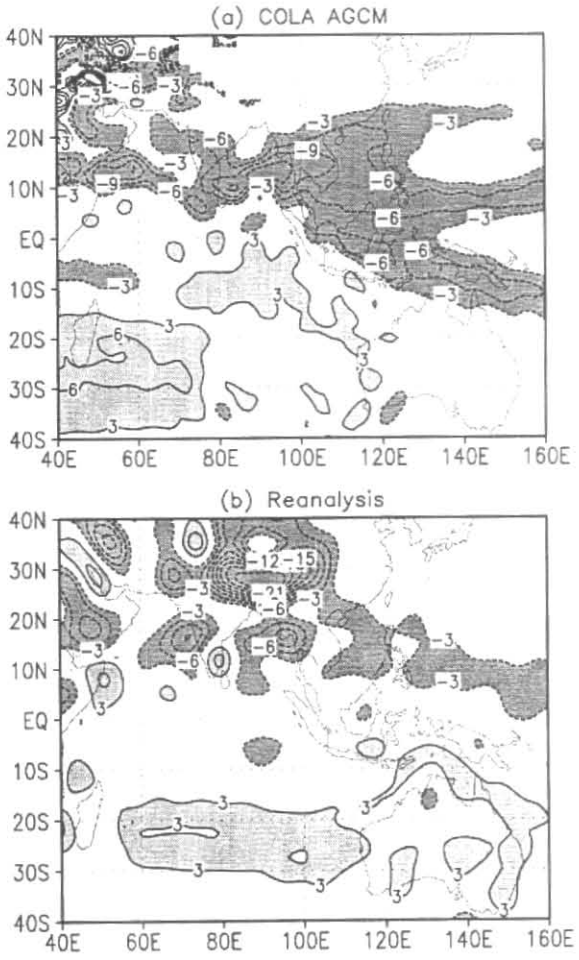

Figs. 7(a&b). JJAS seasonal climatology of the vertical velocity (ω) at 700 hPa for (a) the ensemble mean of COLA GCM integrations and (b) NCEP-NCAR reanalysis. The contour interval is 3 Pa s^{-1}. Positive contours > 3 are in light shade and negative contours < -3 are in dark shade

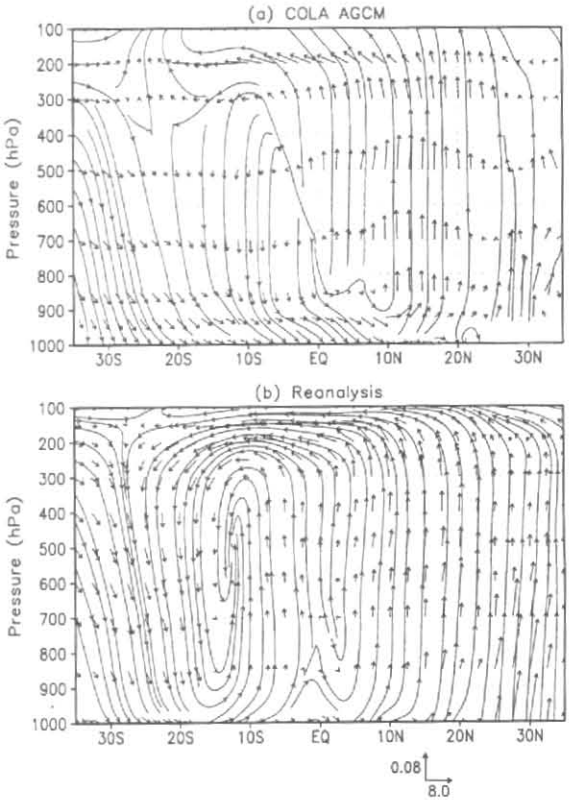

Figs. 8(a&b). JJAS seasonal climatology of the regional zonal mean meridional circulation. Latitude height section of (V, -ω) averaged over 70°–110°E for (a) the ensemble mean of COLA GCM integrations and (b) NCEP-NCAR reanalysis. The unit vector in the horizontal direction is 8.0 m s^{-1} and that in the vertical direction is 0.08 Pa s^{-1}. Streamlines are shown in thin lines

the model climatology is similar to the observed climatologies but with more rainfall. However, over the Bay of Bengal, the model produces considerably more rainfall with the location of the maximum being closer to the east coast of south India.

The actual values of the IMR index for JJAS seasonal and annual climatologies are provided in Table 1 for the model's ensemble mean and for the observed IMD, Parthasarathy, Willmott and CMAP data. The model underestimates the JJAS seasonal IMR index by 2.2–2.5 mm day^{-1} compared to the more accurate IMD and Willmott climatologies. The IMR of Parthasarathy is closer to the IMD climatology, but the CMAP climatology differs by more than 1 mm day. The annual climatological IMR index of the model and the observations differ at the most by 0.4 mm day^{-1}.

The JJAS seasonal rainfall climatology for the larger Asian-Australian monsoon region is shown in Fig. 4 for the ensemble mean of the model integrations and for the observed CMAP, NCEP-NCAR reanalysis and MSU datasets. The model and the observations show very little rainfall during JJAS season in the region south of 15°S. Both CMAP and the NCEP-NCAR reanalysis show a large band of maximum rainfall in the 0–20°N belt east of 80°E. A similar band is also present in the model climatology but with much greater intensity. This band is seen as two small maxima in the MSU climatology. Also, a region of maximum rainfall covering 70°–100°E around the equator is present in the CMAP climatology but not in the NCEP-NCAR reanalysis and MSU climatologies. This band is present to some extent in the model climatology but does not extend northward

TABLE 2

JJAS seasonal anomaly of IMR index (mm day^{-1}) for IMD, CMAP and the ensemble mean of COLA GCM integrations

Year	IMD	CMAP	COLA GCM
1979	-1.06	0.07	1.15
1980	0.38	1.15	0.66
1981	0.13	0.17	0.76
1982	-0.83	-0.89	-1.20
1983	0.97	0.47	-0.25
1984	0.00	-0.91	-0.25
1985	-0.63	-0.51	0.50
1986	-0.77	-0.82	-0.39
1987	-1.15	-1.07	-0.16
1988	1.02	0.80	1.09
1989	0.24	-0.52	-0.31
1990	0.59	0.34	-0.83
1991	-0.43	-0.12	0.16
1992	-0.43	-0.45	-0.47
1993	0.49	0.03	-1.20
1994	0.83	0.84	-1.60
1995	-0.09	0.17	0.59
1996	0.17	0.25	0.29
1997	0.27	0.47	0.41
1998	0.30	0.55	1.02

into the Bay of Bengal as in the CMAP climatology. The equatorial rainfall maximum to the south of India is an important feature of the monsoon climatology, and a better estimation of its amplitude and structure is needed to understand monsoon dynamics. The model climatology is an overestimation of the rainfall in this larger region, as revealed by the AAMR index of the monthly climatology presented earlier in Fig. 2(c).

3.4. *Seasonal mean circulation*

The JJAS seasonal climatologies of certain circulation fields simulated by the model are compared

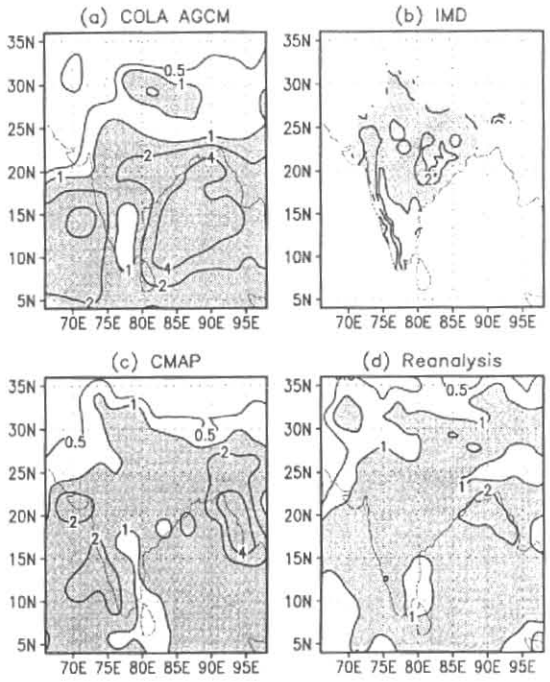

Figs. 9(a-d). Standard deviation of the JJAS seasonal rainfall anomaly for (a) the ensemble mean of COLA GCM integrations, (b) IMD data (c) CMAP, (d) NCEP-NCAR reanalysis. (a, c & d) are based on 1979-98 anomalies and (b) on 1901-70 anomalies. The contours are 0.5, 1.0, 2.0, and 4.0 mm day^{-1}, and contours > 1 are shaded

with those of the NCEP-NCAR reanalysis winds, all based on the period 1979–98. The climatology of the 850 hPa horizontal wind (U, V) of the ensemble mean of the model integrations shown in Fig. 5(a) bears a close resemblance to the reanalysis winds shown in Fig. 5(b). The model climatology reproduces the strong westerlies in the 10°S-20°S band, the cross-equatorial flow, the southwesterly flows in the Arabian Sea and Bay of Bengal remarkably well. The model winds, however, have a higher intensity over the Arabian Sea, the Bay of Bengal and the Phillippines region where the precipitation values were also higher (Fig. 4a). The convergence in the Pacific occurs more to the east in the model than observed.

The climatology of the 200 hPa horizontal winds for the JJAS season is shown in Fig. 6 for the ensemble mean of the model integration and for the reanalysis. The model climatology is once again remarkably close to that of the reanalysis with an easterly jet in the equatorial region and a westerly jet south of 20°S. The only exception is the weaker winds in the model over India and the Bay of Bengal.

TABLE 3

Correlation between observed data and COLA GCM data for precipitation and circulation indices. The indices are JJAS seasonal anomaly for 1979–98. The observed data used are Parthasarathy data for IMR index, CMAP data for EIMR and AAMR indices, and NCEP-NCAR reanalysis for MH and WY indices

Correlation of observed data with	IMR	EIMR	AAMR	MH	WY
Ensemble member 1	0.00	-0.09	0.63	-0.03	0.01
Ensemble member 2	0.07	-0.16	0.71	0.23	-0.07
Ensemble member 3	-0.13	-0.09	0.71	0.03	0.08
Ensemble member 4	-0.12	0.12	0.71	0.20	-0.01
Ensemble member 5	-0.01	-0.04	0.60	0.04	0.03
Ensemble member 6	0.03	0.08	0.68	0.28	-0.07
Ensemble member 7	-0.20	-0.06	0.71	0.03	0.41
Ensemble mean	-0.08	-0.04	0.71	0.15	0.06

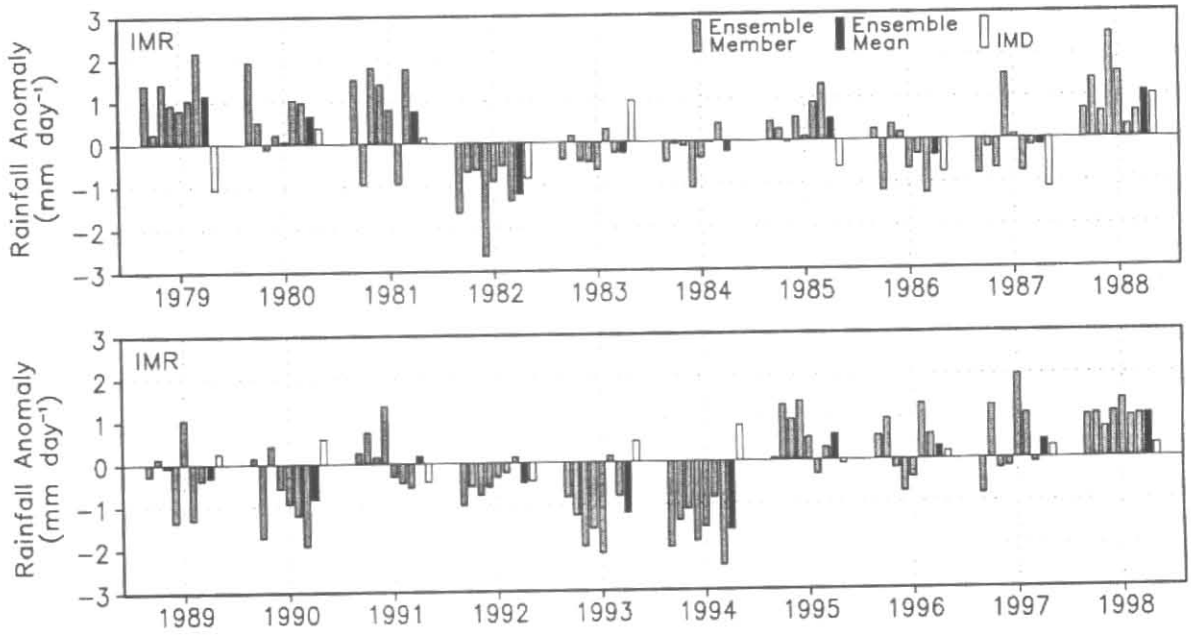

Fig. 10. Time series of JJAS seasonal anomaly of IMR index (mm day^{-1}) for the seven ensemble integrations of COLA GCM, the ensemble mean and the observed IMD data

The climatology of the 700 hPa vertical velocity (ω) for the ensemble mean of the model and the reanalysis is shown in Fig. 7. Unlike the horizontal winds, the model climatology of ω at 700 hPa shows considerable differences from the reanalysis climatology. The branches of the model's descending motion in the Southern Hemisphere are in quite different locations. The ascending branch in the model over the Pacific is much broader and has stronger vertical velocities than the reanalysis. The maxima of the model's vertical velocity over the Arabian Sea and the Bay of Bengal are also in different locations compared to the reanalysis vertical

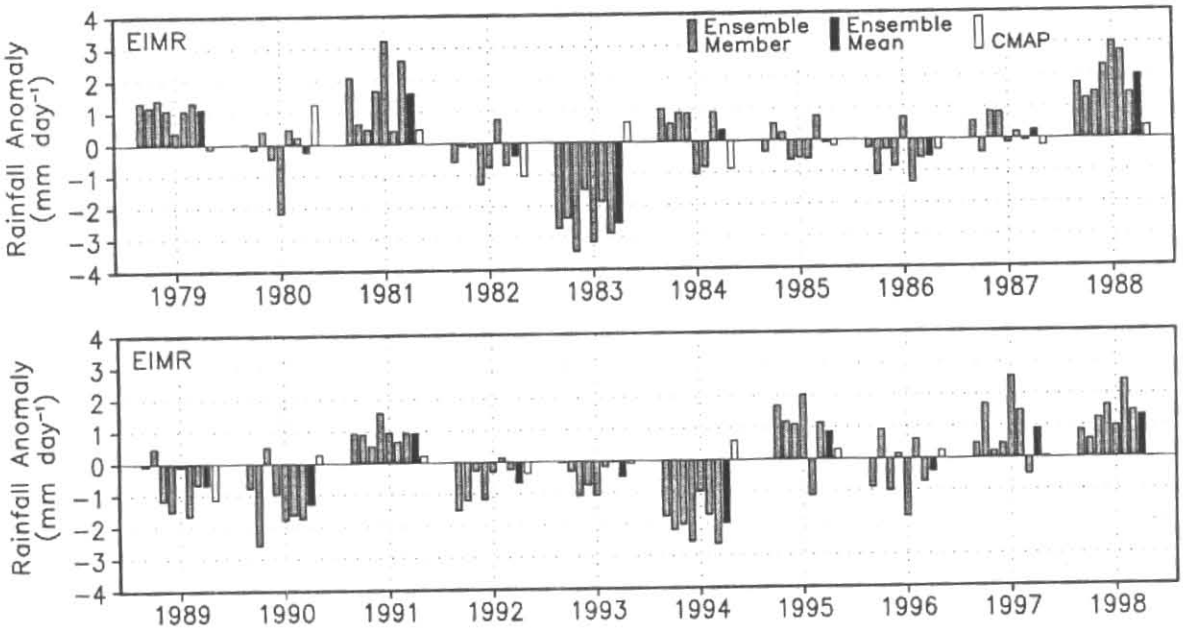

Fig. 11. Time series of JJAS seasonal anomaly of EIMR index (mm day^{-1}) for the seven ensemble integrations of COLA GCM, the ensemble mean and the observed CMAP data

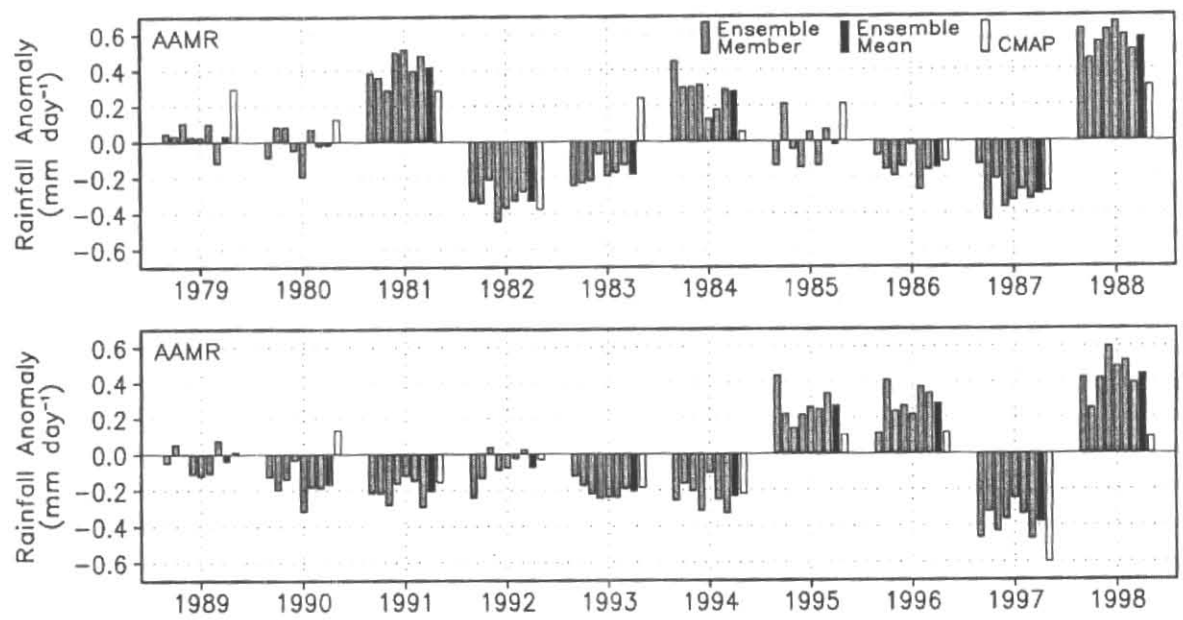

Fig. 12. Time series of JJAS seasonal anomaly of AAMR index (mm day^{-1}) for the seven ensemble integrations of COLA GCM, the ensemble mean and the observed CMAP data

velocity. The branches of the vertical motion in both the model climatology and the reanalysis seem to correspond with the precipitation climatology in Fig. 4.

In order to obtain a three-dimensional structure of the circulation over the Indian monsoon region, the JJAS climatology of the zonal mean circulation averaged over the monsoon sector is presented in Fig. 8. The latitude-height section of the wind vector (V, $-\omega$) averaged over 70°–110°E for the ensemble mean of the model integrations and for the reanalysis are compared in Fig. 8. The observed meridional circulation consists of a large cell with a broad region of ascending motion between 10°S and 25°N and descending motion to the south. The model climatology shows a meridional cell with stronger ascending motion only in the region 10°–15°N, roughly corresponding to the strong precipitation zone over the Bay of Bengal (Fig. 4a). The descending branch of the model's meridional cell south of the equator is considerably weaker than that of the reanalysis.

4. Interannual Variability

The interannual variability of the model is studied by analyzing the JJAS seasonal anomalies of precipitation and circulation fields and by comparing to observations. The spread in the ensemble simulation by the model is also studied, and quantitative analysis of the variability due to internal dynamics and external (SST) forcing is also performed.

4.1. *Standard deviation of precipitation*

The standard deviation of JJAS seasonal precipitation anomalies of the model's ensemble mean and of the observed IMD, CMAP data and the NCEP-NCAR reanalysis is presented in Fig. 9. In general, the model-simulated variability is considerably larger than the corresponding observations. The IMD precipitation (Fig. 9b), covering a long period of time, shows large standard deviation over the Western Ghats and a maximum over the central India, the same locations as those of maximum climatological mean values as seen in Fig. 3(b). Both these features are not reproduced by either the CMAP or the reanalysis data Figs. 9 (c & d). The standard deviation of the model precipitation (Fig. 9a) shows a maximum that is southeast of the location of the central Indian maximum in the IMD data. The standard deviation over the Western Ghats in the model simulation is smaller compared to the IMD data while it is much larger over the entire Bay of Bengal compared to CMAP or reanalysis data.

4.2. *Rainfall indices*

In order to examine the interannual variability of the rainfall in different monsoon regions, the three rainfall indices, IMR, EIMR and AAMR, as defined in section 3.2, for the JJAS seasonal rainfall anomalies were calculated for 1979–98 data from model integrations and observations. The IMR index, which averages the rainfall over land region of India, is shown in Fig. 10 for the seven members of the model ensemble integrations, the ensemble mean and the observed Parthasarathy data. The correlations between the model time series and the observed time series are given in Table 3. From Fig. 10, it is clear that the IMR index of the model's individual ensemble members and the ensemble mean have poor correspondence with the observed IMR index. The correlation between the model and observed time series is quite small for all the ensemble integrations (Table 3). It is remarkable that, for 15 out of 20 years, at least 5 members of the ensemble have the same sign as the ensemble mean; however, the ensemble mean rainfall anomalies are not in agreement with the observed rainfall anomalies for a large number of years.

The EIMR index, which averages the rainfall over India and the surrounding oceanic regions, is plotted in Fig. 11 for the model ensemble integrations and for the observed CMAP data, and the correlations between the observed and model time series are given in Table 3. The correspondence between the model and observed time series of the EIMR index is just as poor as for the IMR index. The time series of the AAMR index for the model integrations and for the observed CMAP data is shown in Fig. 12, and the correlations between the two time series are given in Table 3. The AAMR index averages the rainfall over a large region with a considerable part of Pacific and Indian Oceans. From Fig. 12, it is clear that the model's AAMR index has good correspondence with the observed AAMR index. For most years, the spread among the ensemble members is quite small. The correlation between the model index and the CMAP index is quite good, with correlations ranging from 0.6 to 0.71 for the ensemble members and ensemble mean (Table 3). This suggests that the model is able to capture the boundary forced interannual variability of rainfall only for large spatial averages.

4.3. *Circulation indices*

For further diagnostic investigation of the model's simulation of the monsoon, two circulation indices were used for comparing the interannual variability of the model and observations. The first index used is the Monsoon Hadley (MH) index defined as the meridional

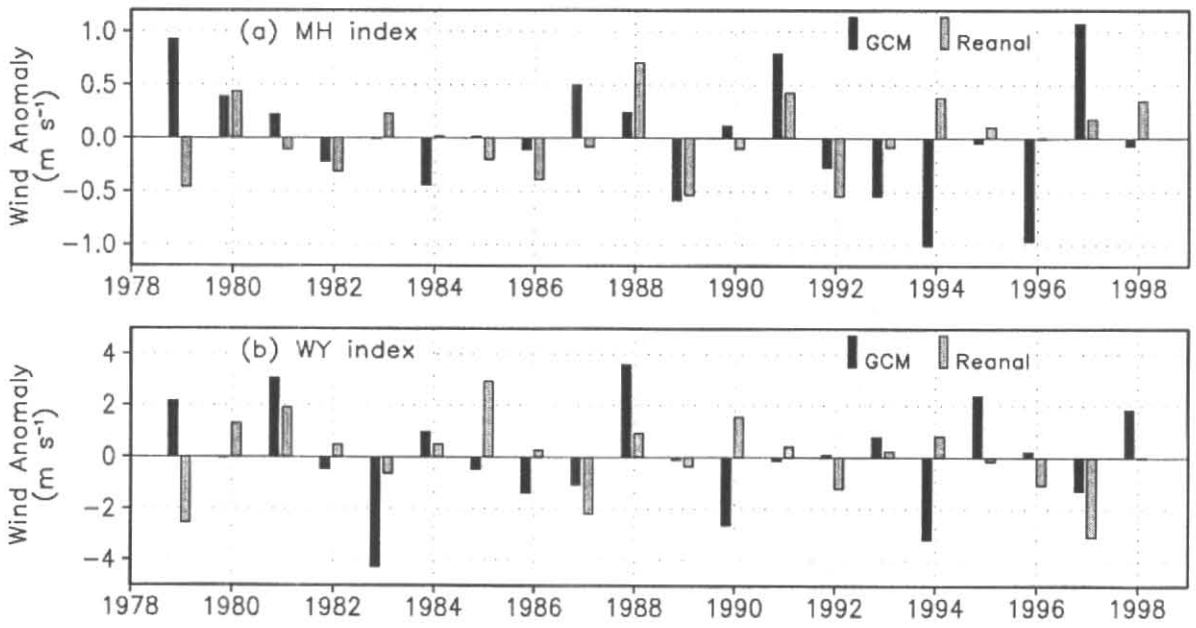

Figs. 13(a&b). Time series of JJAS seasonal anomaly of (a) MH index (m s^{-1}) and (b) WY index (m s^{-1}) for the ensemble mean of COLA GCM integrations and for the NCEP-NCAR reanalysis

wind-shear anomaly (V between 850 hPa and 200 hPa) averaged over (70°–110°E, 10°–30°N) (Goswami *et al.* 1999). The MH index averages over the same area as the EIMR index, and is representative of the regional Hadley circulation driven by the gradient of diabatic heating associated with the variations of the EIMR. The second index used is the Webster-Yang (WY) index defined as the zonal wind-shear anomaly (U at 850 hPa - U at 200 hPa) averaged over (40°–110°E, 0°–20°N) (Webster and Yang 1992). The WY index is more closely associated with the convective activity over the western Pacific region and is more representative of the planetary-scale variations associated with the Indian summer monsoon.

The MH and WY indices were calculated for 1979–98 JJAS seasonal anomalies for the ensemble mean of the model integrations and for the NCEP-NCAR reanalysis data. The time series of the MH index and WY index are shown in Figs. 13 (a & b), respectively. For both indices, the correspondence between the model's ensemble mean and the reanalysis time series is quite poor. This is further confirmed in the correlations between the model time series and reanalysis time series for the two indices given in Table 3. As seen in Table 3, all the individual members of the ensemble as well as ensemble mean have very low correlations with the observed reanalysis indices. It will be shown in section 5 that the correlations among the model-simulated rainfall and the model-simulated circulation indices are quite comparable to similar correlations for observations.

4.4. *Internal variability and SST-forced variability*

Although the interannual variability of the model simulation does not compare well with that of the observations, members of the ensemble do not show large spread especially for large scale rainfall and circulation indices. The seven ensemble integrations provide a way to estimate the relative contributions of internal variability and SST-forced variability. The method used for such quantitative estimate of the internal and SST-forced variability follows the method used by Rowell *et al.* (1995). The total variance of the seasonal mean indices of the model simulation are assumed to consist of variance due to SST forcing and variance due to internal dynamics. The ensemble mean variance with an appropriate correction for sampling is assumed to be the SST-forced variance.

The partition of the total variance of the IMR, EIMR and AAMR indices of the JJAS seasonal anomalies for 1979–98 was estimated using the seven ensemble integrations of the model. The model variances are presented in Table 4, along with the total variances of the

TABLE 4

Variances of precipitation indices for model and observed data. The indices are JJAS seasonal anomalies for 1979–98 with seven ensemble integrations of the model and CMAP dataset for observations

Index	Observed variance $(mm\ day^{-1})^2$	Model's Total variance $(mm\ day^{-1})^2$	Model's Internal variance/Total variance (%)	Model's SST variance / Total variance (%)
IMR	0.41	0.57	47	53
EIMR	0.34	1.28	31	69
AAMR	0.06	0.08	11	89

indices from the NCEP-NCAR reanalysis data. Table 4 shows that SST-forced variability accounts for more than half of the total variance for all the regions over which the indices are averaged. For the Indian land region (IMR index), the internal variability is quite close to the SST-forced variability. For the larger Asian-Australian region (AAMR index), the SST-forced variability provides most of the variance. The total variance of the model is comparable to the observed variance for the IMR and AAMR regions. However, the model variance is quite high for the EIMR region, perhaps because of the high variability of rainfall over the Bay of Bengal.

4.5. *Composites*

The previous discussion shows that the interannual variability of the model's precipitation and circulation have poor correspondence to the observed variability over the Indian region although the model climatology is in reasonable agreement with the observations. In order to examine whether the internal consistency between model-simulated circulation and rainfall is in agreement with the observations, two different composites were calculated from the model's ensemble mean for JJAS 1979–98. One composite was based on years of strong and weak monsoons over India as determined by the IMR index from observations (CMAP) while the other composite was based on the model simulated IMR index. The strong (weak) years both for observations and model are defined to be those when the IMR index is greater (less) than one positive (negative) standard deviation unit. With this definition, each composite consisted of three to four years; however, strong/weak years for the model do not necessarily correspond to strong/weak years for observations.

The difference between the strong and weak composites of the precipitation anomalies of the model's ensemble mean for the model's composite years is shown in Fig. 14(a). A similar composite difference for the CMAP precipitation anomalies based on the observed IMR composite years is shown in Fig. 14(b). The corresponding difference composites for the horizontal wind anomalies at 850 hPa are shown in Fig. 14 (c & d), respectively. Figs. 14 (b & d) have little resemblance to the corresponding model composites based on observed IMR composite years as the strong/weak years are quite different in observations and model stimulations. However, from Figs. 14 (a-d), it is seen that the precipitation and wind anomalies of the model composites with model's strong/weak years are quite comparable to the observed ones over the Indian region. Therefore, the model seems to simulate consistent precipitation and wind anomaly patterns for strong and weak monsoon years. However, the model is unable to forecast the observed rainfall anomalies even when observed SST was prescribed.

5. Summary and Discussion

An ensemble of seven integrations of the COLA AGCM has been performed with prescribed observed SST for the period 1979–98, and the model-simulated monsoon circulation and rainfall have been compared with observations. Although the seasonal mean climatological circulation, and also precipitation to some extent, have been reasonably well simulated, the model-simulated interannual variability of the Indian monsoon rainfall has no correspondence to the observed variability. The model's annual cycle of the rainfall shows an early onset of the monsoon with lower rainfall over the land region of India compared to observations, and heavy rainfall over the Bay of Bengal and the Arabian Sea during the summer months. The climatological mean rainfall simulated by the model for the JJAS season appears to have reasonable intensity over India except for the shift in the locations of the maxima over central India and the Western Ghats. However, the rainfall over the Bay of Bengal and Arabian

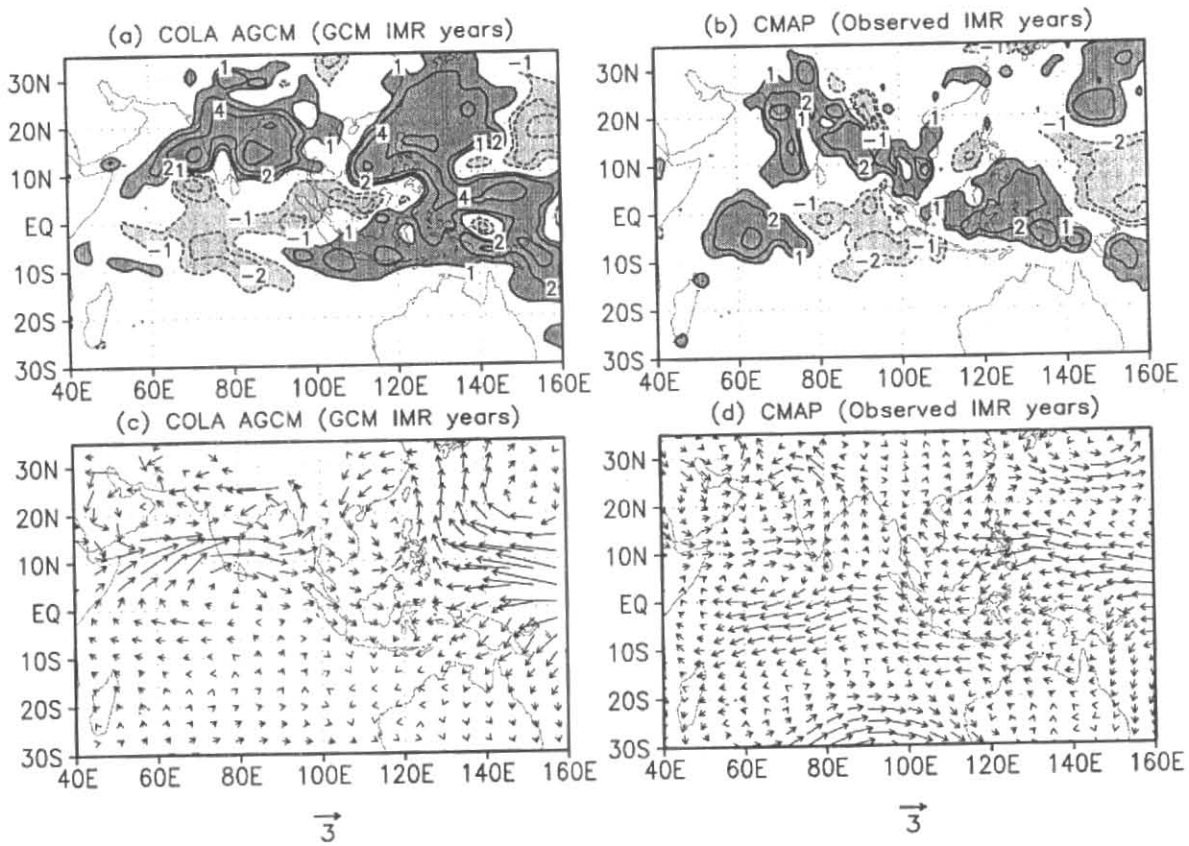

Figs. 14(a-d). Composite difference between strong and weak monsoon years for JJAS seasonal anomaly of precipitation during 1979–1998 for (a) ensemble mean of COLA GCM integrations and (b) CMAP data. The contours are -2, -1, 1, 2 and 4 mm day^{-1}. Positive contours are in dark shade and negative contours are in light shade. Similar composite difference of (U, V) at 850 hPa for (c) ensemble mean of COLA GCM integrations and (d) NCEP-NCAR reanalysis. The unit vector is 3 m s^{-1}. The strong and weak years in (a) and (c) are based on the IMR index of the ensemble mean of the COLA GCM integrations and those in (b & d) are based on the observed IMR index

Sea are quite high, while the equatorial rainfall maximum south of India is not well simulated. Although there are differences in the mean rainfall over other parts of the Asian-Australian region between the model and observations, the rainfall averaged over a large region (AAMR) shows good correspondence. The general features of the observed climatological mean circulation has been captured reasonably well by the model. However, the model produces stronger winds in the southwesterly flow over India at 850 hPa compared to observations and weaker winds over India and Bay of Bengal at 200 hPa.

The standard deviation of the JJAS seasonal mean rainfall in the model simulation has realistic values over the land region of India, but with a shift in the location of the maximum over central India, lower values over the Western Ghats and higher values over the Bay of Bengal compared to observations. The JJAS seasonal anomalies of the rainfall over India, as estimated by the IMR and EIMR indices, have very little correlation with the observed anomalies for the period 1979–98. The circulation anomalies, as estimated by the MH and WY indices, show similarly poor correlation between the model simulation and observations. The rainfall averaged over a larger region, as estimated by the AAMR index, shows very good correlation with model simulations.

Although the model-simulated interannual variability of rainfall and circulation is not in agreement with observed variability, the model shows remarkable reproducibility in that several members of the ensemble are similar to the ensemble mean. An estimation of the partition of the variance of the model-simulated rainfall shows that the SST-forced component of the variance is dominant over the component due to internal dynamics.

TABLE 5

Cross correlation between different rainfall and circulation indices for JJAS seasonal anomaly of 1979–98. The upper triangle (bold) is for observations and the lower triangle is for the model ensemble mean

Index	IMR	EIMR	Nino3	MH	WY
IMR	1.00	**0.49**	**-0.26**	**0.60**	**0.25**
EIMR	0.75	1.00	**-0.05**	**0.66**	**0.19**
Nino3	-0.21	-0.16	1.00	**-0.12**	**-0.62**
MH	0.55	0.52	0.43	1.00	**0.20**
WY	0.64	0.86	-0.47	0.16	1.00

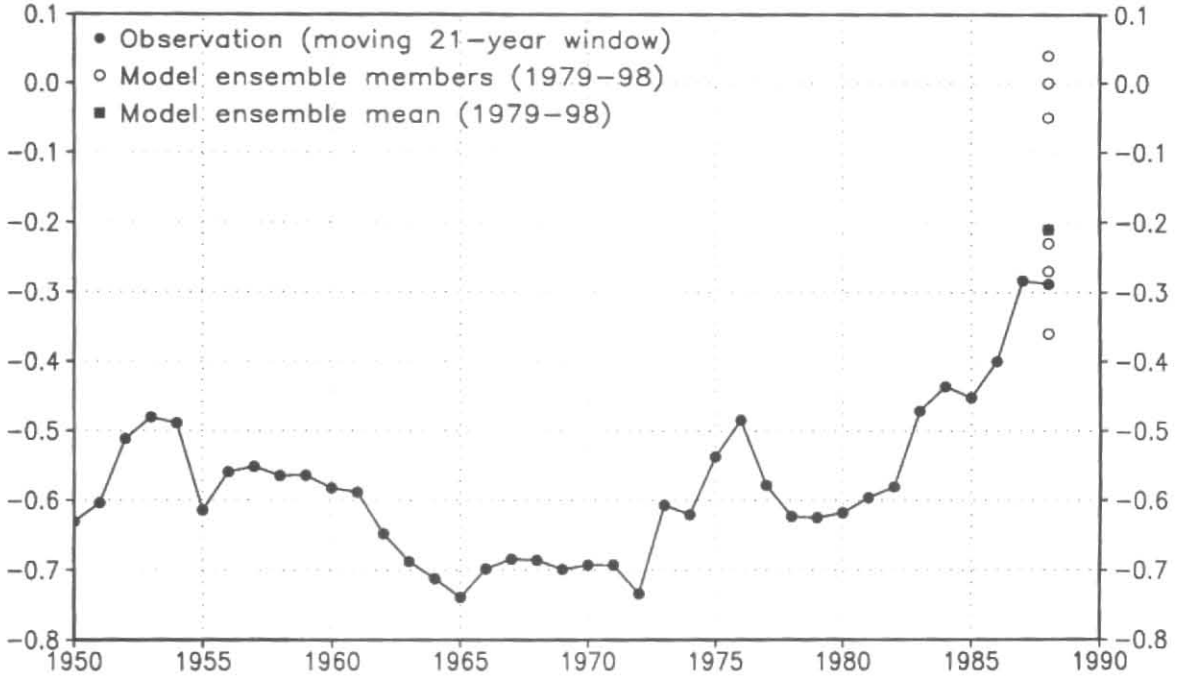

Fig. 15. Correlation between Nino3 index of SST anomalies and IMR index for observed data in a 21-year moving window during 1940-1998 (filled circle), for the model ensemble members during a single period 1979-98 (unfilled circle) and for the model ensemble mean for 1979-98 (filled rectangle) (see text for details)

These results are consistent with correlations between the circulation indices and precipitation indices of the model simulation. For example, the WY index, which represents the planetary scale circulation due to SST forcing, has high correlation with both IMR and EIMR indices in the model.

Table 5 provides correlations among several rainfall and circulation indices for both the model and observations. The Nino3 index (SST anomaly averaged over 150°–90°W, 5°S–5°N) for the JJAS season was calculated using the SST data from the Hadley Centre for Climate Prediction and Research. It is interesting to note

that when the correlations are calculated for the model's circulation and rainfall indices, they are quite comparable (sometimes even higher) to the corresponding correlations using observations. This suggests that the internal consistency between circulation and rainfall is well simulated by the model. However, when model simulations are treated as forecasts and compared to actual observations, there is practically no skill in the forecasts. There are three possible interpretations of this result: (1) the global boundary conditions of SST have no significant effect on the summer monsoon rainfall over India; (2) the model is not accurate enough to capture the influence of SST on rainfall over India and this is as good as it can be expected for this model; and (3) other boundary conditions over land (soil wetness, snow, etc.) are important but not treated here properly. The reproducibility of the model simulations (shown in Figs. 10, 11 and 12) suggests that the SST-forced response is significant because the internal dynamics of the model is not able to degrade the predictability. However, the actual verification of the model rainfall compared to observations is poor. We have not performed any experiments to test the importance of the land surface processes.

Fig. 15 gives the correlation coefficient between the observed SST over the Nino3 region and the observed Indian summer monsoon rainfall. Each filled circle in Fig. 15 represents the correlation for the 21-year period centered at the year for which the filled circle is plotted. The last filled circle corresponds to the period 1978–98. The open circles and the filled square correspond to similar correlation between the observed SST over the Nino 3 region and the model-simulated summer monsoon rainfall over India. The seven open circles correspond to the seven members of the ensemble, and the filled square corresponds to the ensemble mean (correlation of one of the ensemble members happens to be almost equal to that of the ensemble mean). The most remarkable feature of Fig. 15 is a gradual degradation of the Nino3-monsoon rainfall correlation during the last 30 years of the observations. The observed correlation is minimum for the latest 21-year period. The correlations for the model-simulated rainfall are also quite low and in agreement with the observations. It is not understand why the Nino3-monsoon relation has degraded in the last 20 years, perhaps the extension of the model integrations for 50–100 year period may be necessary to address the question further.

Acknowledgements

This work was supported by grants from the National Science Foundation (ATM-9814295), the National Oceanic and Atmospheric Administration (NA96-GP0056), and the National Aeronautics and Space Administration (NAG5-8202).

References

Goswami, B. N., Krishnamurthy, V. and Annamalai, H., 1999, "A broad-scale circulation index for the interannual variability of the Indian summer monsoon", *Quart. J. Roy. Meteor. Soc.*, **125,** 611–633.

Hartmann, D. L., and Michelsen, M. L., 1989, "Intraseasonal periodicities in Indian rainfall", *J. Atmos. Sci.*, **46**, 2838–2862.

Kalnay, E. and Coauthors, 1996, "The NCEP/NCAR 40-year Reanalysis Project", *Bull. Amer. Soc.*, **77,** 437–471.

Kinter III, J. L., DeWitt, D., Dirmeyer, P. A., Fennessy, M. J., Kirtman, B. P., Marx, L., Schneider, E. K., Shukla, J. and Straus, D. M., 1997, "The COLA atmospheric-biosphere general circulation model. Volume 1: Formulation", *COLA Tech. Report 51*, 46 pp, Center for Ocean-Land-Atmosphere Studies, Calverton, Maryland.

Krishnamurthy, V. and Shukla, J., 1999, "Intraseasonal and interannual variability of rainfall over India", *COLA Tech. Report 69*, 34 pp., Center for Ocean-Land-Atmosphere Studies, Calverton, Maryland.

Legates, D. R. and Willmott, C. J., 1990, "Mean seasonal and spatial variability in gauge-corrected, global precipitation", *Int. J. Climatol.*, **10,** 111–127.

NMC Development Division staff, 1988, "Research version of the medium range forecast model", *NMC Documentation Series No. 1*, Development Division, NMC, Washington DC.

Parthasarathy, B., Munot, A. A. and Kothawale, D. R., 1995, "Monthly and seasonal rainfall series for all India, homogeneous regions and meteorological subdivisions: 1871–1994", *Research Report No. RR-065*, 113 pp, Indian Institute of Tropical Meteorology, Pune, India.

Rowell, D. P., Folland, C. K., Maskell, K. and Ward, M. N., 1995, "Variability of summer rainfall over tropical north Africa (1906-92): Observations and modelling", *Quart. J. Roy. Meteor. Soc.*, **121,** 669–704.

Shukla, J., 1998, "Predictability in the midst of chaos: A scientific basis for climate forecasting", *Science*, **282,** 728-731.

Shukla, J., Paolino, D. A., Straus, D. M., DeWitt, D., Fennessy, M., Kinter, J. L., Marx, L. and Mo, R., 1999, "Dynamical seasonal predictions with the COLA atmospheric model", *COLA Tech. Report 67*, 42 pp, Center for Ocean-Land-Atmosphere Studies, Calverton, Maryland.

Spencer, R. W., 1993, "Global oceanic precipitation from the MSU during 1979-91 and comparisons to other climatologies", *J. Climate*, **6,** 1301–1326.

Sperber, K. R. and Palmer, T. N., 1996, "Interannual tropical rainfall variability in general circulation model simulations associated with the Atmospheric Model Intercomparison Project", *J. Climate*, **9**, 2727–2750.

Webster, P. J., Magaña, V. O., Palmer, T. N., Shukla, J., Tomas, R. A., Yanai, M. and Yasunari, T., 1998, "Monsoons: Processes, predictability, and the prospects for prediction", *J. Geophys. Res.*, **103**, 14451–14510.

Webster, P. J. and Yang, S., 1992, "Monsoon and ENSO: Selectively interactive systems", *Quart. J. Roy. Meteor. Soc.*, **118**, 877–926.

Xie, P. and Arkin, P. A., 1996, "Analyses of global monthly precipitation using gauge observations, satellite estimates and numerical model predictions", *J. Climate*, **9**, 840–858.